Continuous measurement of fiber reinforcement permeability in the thickness direction: Experimental technique and validation

P. Ouagne, Tariq Ouahbi, Chung Hae Park, Joël Bréard, Abdelghani Saouab

Continuous measurement of fiber reinforcement permeability in the thickness direction: Experimental technique and validation

Pierre Ouagne[1], Tariq Ouahbi[2], Chung Hae Park[2*], Joël Bréard[2], Abdelghani Saouab[2]

1. Laboratoire PRISME, University of Orléans, 8 rue Leonard de Vinci, 45072 Orléans, France

2. Laboratoire d'Ondes et Milieux Complexes, UMR 6294 CNRS, University of Le Havre, 53 rue de Prony, BP 540, 76058 Le Havre, France

*To whom correspondence should be addressed: chung-hae.park@univ-lehavre.fr

Tel: +33 2 32 21 71 21, Fax: +33 2 35 21 71 98

Abstract

It is an important topic to measure the through-thickness permeability of fiber reinforcements as the resin flow in the thickness direction is widely employed in many composites manufacturing techniques. Continuous techniques for the permeability measurement by simultaneous fabric compaction and liquid flow have been recently proposed as an alternative way to the tedious and laborious conventional permeability measurement techniques. In spite of their efficiencies, these continuous techniques have some limits if the fabric compaction speed or flow rate is relatively great. To address this issue, a new equation for the permeability estimation is proposed. Parametric studies are performed to investigate the influences of the experimental conditions on the validity of the continuous technique. A dimensionless number is proposed as a measure of the relative error of the continuous technique.

Key words: A. Fabrics/textiles; A. Polymer-matrix composites (PMCs); E. Resin transfer molding (RTM); E. Resin flow; Permeability

1. Introduction

Liquid composite molding (LCM) processes such as the resin transfer molding (RTM) process and the structural reaction injection molding (SRIM) process are widely adopted to manufacture complex structural parts at a relatively low cost in the aeronautic and automotive industries. The basic principle of these processes is the resin impregnation into dry fiber reinforcement and this phenomenon is generally modeled by Darcy's law [1]. The resin impregnation becomes more difficult in the case of large part manufacturing, because the resin flow path becomes long and the resin flow velocity drops to a small value. Hence, in some LCM processes such as the vacuum assisted resin transfer molding (VARTM) process and the Seeman composite resin infusion molding process (SCRIMP), high permeability layers (HPL) or distribution media (DM) may be integrated into the preform stack to deal with this problem [2-4]. The resin is quickly impregnated through the HPL or DM and then the resin flows into the fiber reinforcement in the through-thickness direction. Because most composite structures have smaller dimensions in the thickness direction than in the longitudinal directions, the flow path can be greatly reduced and the resin impregnation can be facilitated. This principle is also adopted in the resin film infusion (RFI) process.

In this context, the permeability of reinforcement is a key parameter to influence the resin flow as is defined by Darcy's law.

$$u_D = \frac{Q}{A} = -\frac{K}{\mu}\nabla P \tag{1}$$

where u_D is the volume averaged velocity, Q is the flow rate, A is the cross section, K is the permeability, μ is the resin viscosity and P is the resin pressure. Permeability is represented by a three-dimensional tensor as it depends on the direction [5-6].

Two permeability values are used to characterize fiber reinforcements [7]. The first one is called unsaturated permeability. It is measured by monitoring the flow front advancement as a function of time under a given pressure gradient in the transient resin flow [5-7]. The other one is referred as saturated permeability. It is obtained by measuring the pressure gradient under a given flow rate during the steady state flow in the fully impregnated reinforcement [7]. As permeability is a reinforcement property which is independent of resin properties and processing conditions, the unsaturated permeability and the saturated permeability for a specific reinforcement should be identical. In the literature, however, the ratio of unsaturated permeability to saturated permeability has been reported to be ¼ to 4 by experimental measurements [8-9]. The main reasons for the difference between the unsaturated permeability and the saturated permeability have been assumed to be the void generation and the flow induced deformation of fiber reinforcements. In this work, this issue is not addressed and only the saturated permeability is discussed.

In general, the permeability is expressed in terms of fiber volume fraction such as in the Kozeny-Carman equation. To obtain a relationship between fiber volume fraction and permeability, it is a usual way to obtain a single set of fiber volume fraction and permeability, by fixing fiber volume fraction and measuring flow rate and pressure drop to evaluate a permeability value. Then, this procedure is repeated for different values of fiber volume fraction to obtain a number of data points which will be used to fit a pre-assumed mathematical equation. In this paper, we call this method “discrete method” because we obtain a series of discrete values of fiber volume fraction and permeability (Figure 1(a)). Hence, a number of measurements are needed and the accuracy of measurement is improved as the number of data points is increased. This method,

however, is tedious and needs a long time. As an alternative way, some researchers proposed to measure the permeability while fiber reinforcement is continuously compacted [10-14]. A stack of fiber reinforcement layers is placed between two rigid tools and is compressed by a motion of one of the rigid tools (Figure 1(b)). The change of the gap between the upper tool and the lower tool induces a change of fiber volume fraction. At the same time, the pressure differential or flow rate is measured as a function of time while the fabric is compressed. The gap height can be converted into the fiber volume fraction and the pressure difference or flow rate is used to obtain the permeability by using Darcy's law, at each instant, during the reinforcement compression. In the current paper, this method is called "continuous method" because the reinforcement is continuously compressed. In this way, it can also be assumed that the data appears to be continuous if the resolution of data acquisition is sufficiently fine. The advantage of the continuous methods over the discrete methods is the reduction of the number of measurements and of the time to work. A relationship between fiber volume fraction and permeability can be obtained by a single measurement in the continuous methods, whereas many measurements are needed in the discrete methods.

Two kinds of continuous methods are found in the literature. In the first method, a saturated fabric stack is squeezed by rigid platens without any external liquid flow. In this case, the liquid flow is induced only by the platen velocity. In the second method, a fabric stack is compacted while it is submitted to an external liquid flow. In this case, the liquid flow is induced both by the platen motion and by the external liquid flow applied to the fabric stack.

The continuous methods have been used to identify the in-plane permeabilities [10-11]. The resin flow takes place in the longitudinal direction while the fabric is compressed in

the thickness direction. Not only the permeabilities of isotropic preforms but also the permeabilities of anisotropic preforms can be obtained once the ratio of two principal in-plane permeabilities is known [11]. Because the anisotropic ratio may depend on fiber volume fraction, however, a significant number of extra measurements may be required.

Scholz et al. proposed a continuous method to measure through-thickness permeability by applying a flow of liquid or gas in the thickness direction [12]. They found that the permeability values obtained by injecting a gas or liquid showed close agreements with each other. However, the permeability values obtained by the continuous method were not compared with those obtained by the discrete method. Hence, the reliability of the continuous method was still questionable. Ouagne and Bréard used a similar experimental technique and showed that the permeability values obtained by the continuous method were close to those obtained by the discrete method, if the compression speed was sufficiently low [13]. Using the same experimental device, they found that the difference between the permeability values obtained by the continuous method and by the discrete method could be significant depending on the experimental condition such as the fabric compaction speed and the flow rate [14].

In this work, the reasons for the discrepancy between the continuous method and the discrete method are analyzed, and a new equation for the permeability evaluation by the continuous method is suggested to address this problem. Then, some experimental results of permeability measurements by the discrete method and by the continuous method are presented for different experimental conditions and for different reinforcements. Finally, the validity of the continuous method is examined by parametric studies for different values of fabric compaction speed and flow rate,

through numerical simulations. A dimensionless number is proposed as a measure of the error in the use of the continuous method.

2. Experimental method

2.1 Experimental device

The device developed in the previous work was used again in the current work [13]. The schematic diagram and the photo view of this device are shown in Figure 2. A brief description of the device is presented in this section and the details can be found in the reference [13]. This device consists of a stainless steel cylindrical pot within which the vertical motion of a piston induces the compaction of the fiber reinforcement which is placed between the lower fixed bronze grid and the upper mobile bronze grid. The motion of the piston controlled by a universal testing machine (Instron 8802) leads to a vertical motion to the upper bronze grid at a pre-assigned constant displacement rate. The lower and upper perforated bronze grids are used to obtain a uniform liquid flux through the fiber reinforcement to be tested. A silicon joint is applied at the perimeter of the test reinforcement to avoid race tracking effects. The actual diameter of the circular test reinforcement submitted to the liquid flow is 100 mm. The test liquid which enters the lower chamber in the cylindrical pot passes through the test reinforcement and leaves the upper chamber through the flow outlet. The liquid flow entering the lower chamber is provided from a six liter syringe which is placed on another universal test machine (Instron 5867) and the flow rate is controlled by the crosshead speed of the universal test machine. A pressure transducer (Entran EPXO-X7) is placed below the lower fixed bronze grid to measure the pressure of the liquid entering the test reinforcement. It is assumed that the pressure loss by the upper and lower perforated

bronze grids is negligible by dint of their highly porous microstructure. It is also assumed that the pressure of the liquid leaving the test reinforcement is close to zero because the flow resistance in the upper chamber is negligible.

2.2 Test materials and experimental conditions

Silicon oil (viscosity: 0.1 Pa·s) was used as a test liquid. As test reinforcements, we used three fiber reinforcements.

A. E glass 5 harness satin weave (areal weight: 620 g/m^2, density: 2.56 g/cm^3)

B. Carbon interlock weave (areal weight: 625 g/m^2, density: 1.74 g/cm^3)

C. Flax random mat (areal weight: 520 g/m^2, density: 1.56 g/cm^3)

The permeabilities of the three reinforcements were measured by the continuous method as well as by the discrete method. In the permeability measurement by the discrete method (see Figure 1 (a)), a fabric stack composed of twenty layers at the same layer angle was placed between the upper and lower bronze grids which were stationary during the liquid flow. Fiber volume fraction was computed as follows.

$$V_f = \frac{M_s N_f}{H \rho_f} \tag{2}$$

where V_f is the fiber volume fraction, M_s is the areal weight of reinforcement, N_f is the number of fabric layers, H is the distance between the bronze grids or the thickness of fabric stack, and ρ_f is the fiber density. While the gap between the bronze grids was fixed, the test liquid flowed through the reinforcement at a pre-assigned constant flow rate (6.7×10^{-7} m^3/s for all the cases) and the pressure at the lower chamber was measured. This procedure was repeated with the same stack of the reinforcement layers for different gap heights between the bronze grids. The measurement of pressure was repeated for various gap heights from a large gap height to a small gap height. Hence,

the permeability values were identified from a low fiber volume fraction to a high fiber volume fraction. Given the type of reinforcement, tests were performed three times and the average value was taken. Hence, three stacks of fabrics were used for each type of reinforcement.

In the continuous measurement of permeability (see Figure 1 (b)), a stack of fabrics was prepared in the same way as was in the discrete method. In this case, however, the upper grid moved downward to compact the fabric stack at a pre-assigned constant speed while the test liquid was passing through the fabric stack at a pre-assigned constant flow rate. The gap height was computed at each instant from the initial gap height and the speed of the upper bronze grid. Once the gap height is known, the fiber volume fraction can be calculated at each instant by Equation (2). The pressure at the lower chamber was measured as a function of time. Consequently, the gap height and the pressure at the lower chamber were obtained as a function of time in the continuous method. For each type of reinforcement, tests were performed three times and a new stack of fabrics was used for a new test. Hence, three stacks of fabrics were prepared for each type of reinforcement.

2.3 Permeability calculation by the discrete method

If it is assumed that the pressure distribution is linear and the pressure gradient is uniform in the reinforcement, the negative pressure gradient can be expressed by the ratio of the pressure drop to the total thickness of the fabric stack (Figure 3 (a)).

$$-\frac{dP}{dz} = \frac{\Delta P}{H} = \frac{P_{in} - P_{out}}{H} \tag{3}$$

where P_{in} is the liquid pressure at the entrance of the fabric stack in the lower chamber and P_{out} is the liquid pressure at the exit of the fabric stack in the upper chamber. The

permeability can be obtained from Darcy's law in terms of the flow rate and the inlet pressure, assuming that the outlet pressure is zero.

$$K_d = \frac{\mu HQ}{P_{in} A} \tag{4}$$

where K_d represents the permeability value obtained by the discrete method.

2.4 Permeability calculation by the continuous method

In the previously mentioned references [12-14], the same equation as was used in the discrete method (Equation (4)) has been applied to evaluate the permeability by the continuous method. It was found, however, that the permeability evaluation by the continuous method was dependent on the fabric compaction speed which was not considered in Equation (4) [14].

To address this issue, two phenomena induced by the fabric compaction are considered: the fiber motion and the non-linear pressure gradient.

In fact, the permeability evaluation by Darcy's law is based on the assumption that the fiber bed is stationary during the liquid flow. If there is a motion of fiber, Darcy's law should be modified considering the fiber velocity. In this case, the relative velocity which is the difference between the liquid velocity and the fiber velocity should be associated with the negative pressure gradient.

$$u_D - u_f = -\frac{K}{\mu} \nabla P \tag{5}$$

where u_f is the fiber velocity. In the continuous method where the fabric stack is compressed by the downward motion of the upper grid, the fiber velocity cannot be ignored. Moreover, the fiber velocity depends on the position of the fiber. For example, the fiber velocity just beneath the upper mobile grid equals to the negative value of the fabric compaction speed whereas the fiber velocity just above the lower fixed grid is

zero (Figure 3 (b)). Hence, we propose to use the half of the negative fabric compaction speed as the mean value of the fiber velocity to evaluate the permeability by the continuous method.

$$K_c = \frac{\mu H}{P_{in}}\left(\frac{Q}{A} + \frac{U_c}{2}\right) \tag{6}$$

where U_c is the fabric compaction speed or the upper mobile grid displacement rate. K_c denotes the permeability obtained by the continuous method. In Equation (6), the thickness of the fabric stack (H) and the inlet pressure (P_{in}) are obtained as a function of time. Consequently, the fiber volume fraction can be calculated from the thickness of the fabric stack by Equation (2) and the permeability (K_c) can be obtained by Equation (6), as a function of time (Figure 1 (b)).

The second problem is the non-linear pressure gradient in the fabric stack under applied fabric compaction and liquid flow (Figure 3 (b)). One of the important assumptions in Equation (3) is that the pressure gradient is uniform and the pressure profile is linear in the reinforcement at each instant. If there is a time dependent change of fiber volume fraction, such as in the vacuum infusion process and the resin film infusion process, the rate of fiber volume fraction should be taken into account in the mass conservation equation. Moreover, the fiber velocity should be considered in Darcy's law as was described in Equation (5). Subsequently, the fiber volume fraction becomes non-uniform in the fabric stack by the fiber motion during the liquid flow and the fabric compaction, and the mass conservation equation in the thickness direction should be modified including the terms representing the volumetric change rate and the fiber velocity [15].

$$\frac{\partial}{\partial z}\left(\frac{K}{\mu}\frac{\partial P}{\partial z}\right) = -\frac{1}{V_f}\left(\frac{\partial V_f}{\partial t} + u_f \frac{\partial V_f}{\partial z}\right) \tag{7}$$

If there is no fiber motion and the fiber volume fraction is uniform, both the terms on the right hand side disappear and the pressure distribution becomes linear. If the fiber velocity is no more negligible or the fiber volume fraction is non-uniform, however, the terms on the right hand side should be considered and the pressure distribution becomes non-linear [15]. In general, the fibers are compacted along the liquid flow and the fiber volume fraction is higher in the downstream (Figure 3 (b)). Therefore, the local permeability becomes lower in the downstream and the global liquid flow is decided by the lowest local permeability in the downstream. Consequently, the permeability values measured in the fabrics with non-uniform fiber volume fraction (e.g. under compaction) appears to be lower than those measured in the fabrics with uniform fiber volume fraction.

In the previous section (1. Introduction), two continuous methods were presented, viz., the squeezing of a saturated fabric stack without external liquid flow and the compaction of a fabric stack under an applied liquid flow. In the first case, the relative velocity due to the fiber motion is an important issue whereas the fiber volume fraction is relatively uniform. In the second case, however, both the relative velocity due to the fiber motion and the non-uniformity of fiber volume fraction should be taken into account to evaluate the permeability.

2.5 Results and discussion

In Figure 4, the permeability values of three different reinforcements measured by the continuous method as well as by the discrete method are presented. In general, permeabilities are plotted in the logarithmic scale against fiber volume fraction. In this way, a great error at high permeability zone (e.g. 10^{-10} m^2) appears to be the same as a

small error at lower permeability zone (e.g. 10^{-14} m^2), because both of them are represented by a single scale with the same length in the vertical axis. Hence, permeabilites are plotted in the linear scale for the accurate comparison of discrepancy, in this work. It should be also kept in mind that there is a unique value of permeability for a given fiber volume fraction and the permeability values obtained by the discrete method are considered as the reference values in this work even though the permeability values obtained by the continuous method are plotted together in the same graph. The objective of this section is to see the relative error of the continuous method compared with the discrete method. To evaluate the permeability values by the continuous method, two equations were used and the results were compared: Equation (4) without fiber velocity and Equation (6) with fiber velocity. Compared with the continuous permeability measurements without considering the fiber velocity (Equation (4) and hollow dots in Figure 4), the continuous permeability measurements considering the fiber velocity (Equation (6) and solid dots in Figure 4) are in closer agreements to the discrete permeability measurements. Even though the discrepancy becomes generally marginal with considering the fabric compaction speed in Equation (6), there is still some difference between the discrete and the continuous methods. From the experimental results, some general conclusions can be drawn.

A. The permeability values obtained by the continuous method are generally lower than the permeability values by the discrete method.

B. The difference between the two methods becomes greater as the fiber volume fraction becomes lower.

C. The difference between the two methods increases as the fabric compaction speed increases.

In the subsequent section, these issues are investigated by parametric studies using numerical simulations of liquid flow and fabric compaction. Then, a dimensionless number is proposed as a measure of error in the continuous method.

3. Validation of the continuous method

3.1 Numerical simulation

In order to investigate the influences of non-uniform fiber volume fraction and fiber velocity on the validity of the continuous method, it is indispensable to observe the distributions of fiber volume fraction and of liquid pressure in the thickness direction during the flow and compression. This experimental observation is difficult to conduct, however, because the thickness of fabric stack is very small. Hence, numerical simulations of fabric deformation and resin flow in mesoscopic or microscopic scale can be attractive approaches [16-18]. Simultaneous simulation of fabric deformation and resin flow is a difficult task, however, because there is a mutual influence between the flow-induced fabric deformation and the permeability alteration by the change of fabric microstructure. Instead, numerical simulations based on the mass conservation and the force equilibrium at a mascroscopic scale may be a practical alternative way [19]. The computer code developed in the previous work has been improved, by considering the fiber velocity, to simulate the liquid flow in the thickness direction and the fiber compaction in the fabric stack as represented in Equation (7) [19]. We need another governing equation to describe the force balance condition.

$$P_{comp} = P + \sigma_f \tag{8}$$

where P_{comp} is the total compaction pressure applied to the fabric stack (to be measured by Instron 8802 connected to the piston on the upper mobile grid) and σ_f is the elastic

stress by fabric deformation. The permeability and the fabric deformation stress can be represented as a function of fiber volume fraction.

$$K = a\left(V_f\right)^b \tag{9}$$

$$\sigma_f = c\left(V_f\right)^d \tag{10}$$

Equation (10) is known as "Toll and Manson" equation which is an empirical relation between fabric compaction stress and fiber volume fraction [20, 21]. In a similar way, the in-plane or transverse permeability values have also been related to fiber volume fraction by using a similar empirical power law model [22].

As boundary conditions, a flow rate and zero fiber velocity are assigned at the lower face of the fabric stack. A fiber velocity which is the negative value of the fabric compaction speed and zero liquid pressure are assigned at the upper face of the fabric stack.

The permeability measurement by the continuous technique was simulated by the computer code. The objective of the numerical simulations was to investigate if the continuous method successfully reproduced the permeability values by the discrete method. Hence, the permeability values by the discrete method were used as input data for the numerical simulations and the permeability values by the continuous methods were the output results of the numerical simulations (Figure 5).

Given the permeability values obtained by the discrete method which were considered as the true permeability values of the reinforcement and the fiber stress values obtained by independent measurements, numerical simulations were performed. The identification procedure of fiber stress model coefficients has been described in the authors' previous work [21]. The model coefficients used in Equations (9) and (10) are listed in Table 1. At each numerical simulation, the inlet pressure was obtained as a

function of time. The thickness of fabric stack was computed from the fabric compaction speed and the initial thickness value. Then, the average fiber volume fraction ($V_{f,ave}$ in Figure 5) was obtained as a function of time by using Equation (2) because the fiber volume fraction was varied with the position. Subsequently, the permeability was computed as a function of time by Equation (6) from the inlet pressure obtained by the numerical simulation and the thickness of the fabric stack. The permeability values for each average fiber volume fraction obtained in this way were considered as the permeability by the continuous method.

3.2 Parametric study

Parametric studies were conducted for the three different reinforcements described in Section 2.2, to investigate the influences of the flow rate and the fabric compaction speed upon the validity of the continuous method.

In the case of the glass satin weave and the carbon interlock weave, the permeability values obtained by the continuous method (i.e. by numerical simulations) were compared with the permeability values obtained by the discrete method for three flow rate values (5×10^{-7} m^3/s, 10^{-6} m^3/s and 2×10^{-6} m^3/s) and for three compaction speed values (0.2 mm/min, 1 mm/min and 5 mm/min). In the case of the flax random mat, higher flow rates (2×10^{-6} m^3/s, 10^{-5} m^3/s and 5×10^{-5} m^3/s) were used because there was little discrepancy for lower flow rates between the permeability values obtained by the continuous method and those obtained by the discrete method.

3.3 Results and discussion

The results of numerical simulations are shown in Figure 6. The relative errors of the permeability values by the continuous method to those obtained by the discrete method are defined by the following relation.

$$Err = \frac{K_d - K_c}{K_d} \tag{11}$$

The same conclusions as were previously drawn in the section 2.5 can be made. Moreover, we can see that there is an influence from the flow rate as well as from the fabric compaction speed. The difference between the continuous method and the discrete method increases as the flow rate increases. As the flow rate or the fabric compaction speed increases, the fabric compaction becomes greater at the downstream. This leads to an increase of fiber volume fraction and the corresponding increase of the flow resistance at the downstream. As a result, the global flow resistance drops, and a lower permeability is obtained in the reinforcement with a non-uniform distribution of fiber volume fraction than in the reinforcement with a uniform distribution of fiber volume fraction. For the same flow rate (2×10^{-6} m^3/s) and the same compaction speed (5 mm/min), in particular, the difference between the permeabilities obtained by the discrete method and by the continuous method was relatively small in the case of the flax random mat (see Figure 6 (g)), whereas they were relatively great in the case of the glass satin weave (see Figure 6 (c)) and the carbon interlock weave (see Figure 6 (f)). In the case of the flax mat, the effect of fabric compaction was relatively small and there was little influence from the flow rate and the fabric compaction speed. This implies that the validity of the continuous method depends on the fabric type, especially the fabric compaction behavior, as well as on the flow rate and the fabric compaction speed. Hence, a dimensionless number is proposed for the quantitative validation of the continuous method. The basic assumption adopted in the discrete method was the linear

pressure profile. For this assumption to be valid, the two terms on the right hand side in Equation (7) should vanish. Equation (7) with two variables, viz. pressure and fiber volume fraction, can be converted into an equation with a single variable of fiber volume fraction, from the force balance condition represented in Equation (8) and the relations for the reinforcement permeability and fiber deformation stress represented by Equations (9) and (10), respectively.

$$-\frac{\partial}{\partial z}\left(\frac{a\left(V_f\right)^b}{\mu}\left(cd\left(V_f\right)^{d-1}\frac{\partial V_f}{\partial z}\right)\right)=-\frac{1}{V_f}\left(\frac{\partial V_f}{\partial t}+u_f\frac{\partial V_f}{\partial z}\right) \tag{12}$$

Then, the governing equation for fiber volume fraction is non-dimensionalized introducing a scaling parameter and dimensionless numbers.

$$V_f^*=\frac{V_f}{V_{f,ave}},\quad z^*=\frac{z}{H},\quad u_f{}^*=u_f\frac{V_{f,ave}}{U_c},\quad t^*=t\frac{Q}{AH} \tag{13}$$

Subsequently, we obtain a dimensionless form of the governing equation.

$$\frac{\partial}{\partial z^*}\left(\left(V_f^*\right)^{b+d-1}\frac{\partial V_f^*}{\partial z^*}\right)=-\frac{\mu bH}{acd\left(V_{f,ave}\right)^{b+d}}\left(\frac{Q}{A}\frac{\partial V_f^*}{\partial t^*}+u_f^*\frac{U_c}{V_{f,ave}}\frac{\partial V_f^*}{\partial z^*}\right) \tag{14}$$

Finally, we can define a dimensionless number to represent a magnitude of the right hand side terms as shown below.

$$\beta=-\frac{\mu bH}{acd\left(V_f\right)^{b+d}}\left(\frac{Q}{A}+\frac{U_c}{V_f}\right) \tag{15}$$

If one plots the numerical relative errors as defined in Equation (11), all the results in Figure 6 can be represented by a single master curve, regardless of reinforcement type, in terms of the dimensionless number defined in Equation (15) (see Figure 7). The numerical relative error increases as the dimensionless number increases. It should be noted that the relative error in the case of the flax random mat is smaller than those in the case of the glass satin weave and the carbon interlock weave for the same compaction speed and the same flow rate because the dimensionless number for the flax mat is smaller than those for the other reinforcements (Figure 8). The increase of the compaction speed and the flow rate results in the increase of the dimensionless number

and in the corresponding increase of the relative error as shown in Figure 7. As the fiber volume fraction decreases, the dimensionless number increases and the relative error increases. It should be noted that the thickness of the fabric stack should be sufficiently small, because the dimensionless number is proportional to the fabric stack thickness. Besides, low viscosity liquid is favorable to reduce relative errors as the dimensionless number is proportional to the liquid viscosity. As a consequence, the experimental conditions in the continuous permeability measurement should be adjusted to minimize relative errors in terms of the dimensionless number considering not only the test conditions such as the flow rate and the fabric compaction speed but also the material properties such as the liquid viscosity and the fabric compaction behavior (viz. elastic fiber stress model).

4. Conclusions

The limit of validity of the continuous permeability methods where the fabric stack is continuously compressed during the liquid flow was investigated in this work. Through the experimental measurements of the permeability in the thickness direction, the discrepancies between the discrete method and the continuous method were observed. To investigate the influences of the experimental test conditions such as the flow rate and the fabric compaction speed, numerical simulations were performed for various conditions. A dimensionless number to quantify the relative error of the continuous method was proposed. It was found that the relative errors can be plotted by a master curve in terms of the proposed dimensionless number regardless of fabric type. From the investigation, it can be concluded that low flow rate, low compression speed, small

thickness of fabric stack and low viscosity liquid are advantageous to reduce relative errors.

In this work, it has been assumed that the permeability values obtained by the discrete method are the referential values. From the definition of the dimensionless number in Equation (15), however, we can see that the error can be significant if the flow rate is great, even though the fabric compaction speed is zero. Therefore, a low flow rate should be applied even in the discrete permeability method, in order to avoid a non-uniform distribution of fiber volume fraction induced by the fiber compaction along the liquid flow.

Acknowledgements

This work has been performed in the framework of the research program "LCM3M / ANR (the French National Research Agency)." The authors would like to appreciate the financial support to this research program from the French ministry of the research and higher education.

References

1. Darcy H. Les fontaines Publiques de la ville de Dijon. Paris: Dalmont, 1856.

2. Han K, Jiang S, Zhang C, Wang B. Flow modeling and simulation of SCRIMP for composites manufacturing; Composites Part A 2000; 31(1): 79-86.

3. Sun X, Li S, Lee LJ. Mold filling analysis in vacuum-assisted resin transfer molding. Part I: SCRIMP based on a high-permeable medium. Polymer Composites 1998; 19(6): 807-817.

4. Ni J, Li S, Sun X, Lee LJ. Mold filling analysis in vacuum-assisted resin transfer molding. Part II: SCRIMP based on grooves. Polymer Composites 1998; 19(6): 818-829.

5. Ahn SH, Lee WI, Springer GS. Measurement of the three-dimensional permeability of fiber preforms using embedded fiber optic sensors. Journal of Composite Materials 1995; 29(6): 714-733.

6. Turner DZ, Hjelmstad KD. Determining the 3D permeability of fibrous media using the Newton method. Composites Part B 2005; 36(8): 609-618.

7. Parnas RS, Flynn KM, Dal-Favero ME. A permeability database for composite manufacturing. Polymer Composites 1997; 18(5): 623-633.

8. Dungan FD, Sastry AM. Saturated and unsaturated polymer flows: microphenomena and modeling. Journal of Composite Materials 2002; 36(13): 1581-1603.

9. Pillai KM, Modeling the unsaturated flow in liquid composite molding processes: a review and some thoughts, Journal of Composite Materials 2004; 38(23): 2097-2118.

10. Buntain MJ, Bickerton S. Compression flow permeability measurement: a continuous technique. Composite Part A 2003; 34(5): 445-457.

11. Comas-Cardona S, Binétruy C, Krawczak P. Unidirectional compression of fibre reinforcements. Part 2: A continuous permeability tensor measurement. Composites Science and Technology 2007; 67(3-4): 638-645.

12. Scholz S, Gillespie Jr JW, Heider D. Measurement of transverse permeability using gaseous and liquid flow. Composites Part A 2007; 38(9): 2034-2040.

13. Ouagne P, Bréard J. Continuous transverse permeability of fibrous media. Composites Part A 2010; 41(1): 22-28.

14. Ouagne P, Bréard J. Influence of the compaction speed on the transverse continuous permeability, The 10th International Conference on Flow Processes in Composite Materials (FPCM10). Ascona, Swiss, July 11-15, 2010.

15. Park CH, Saouab A. Analytical modeling of composite molding by resin infusion with flexible tooling: VARI RFI processes. Journal of Composite Materials 2009; 43(18): 1877-1900.

16. Charmetant A, Vidal-Sallé E, Boisse P. Hyperelastic modelling for mesoscopic analyses of composite reinforcements, Composites Science and Technology 2011; 71(14): 1623-1631.

17. De Luycker E, Morestin F, Boisse P, Marsal D. Simulation of 3D interlock composite preforming, Composite Structures 2009; 88(4): 615-623.

18. Silva L, Puaux G, Vincent M, Laure P. A monolithic finite element approach to compute permeability at microscopic scales in LCM processes, International Journal of Material Forming 2010; 3(s1): 619-622.

19. Ouahbi T, Saouab A, Bréard J, Ouagne P, Chatel P. Modeling of hydro-mechanical coupling in infusion processes. Composites Part A 2007; 38(7): 1646-1654.

20. Toll S, Manson JAE. An analysis of the compressibility of fiber assemblies. Proceeding of the sixth International Conference on Fiber-Reinforced Composites, Institute of Materials, Newcastle upon Tyne, UK, 1994: 25/1-25/10.

21. Ouagne P, Bréard J, Ouahbi T, Saouab A, Park CH. Hydro-Mechanical Loading and Compressibility of Fibrous Media for Resin Infusion Processes, International Journal of Materials Forming 2010; 3: 1287-1294.

22. Gauvin R, Clerk P, Lemenn Y, Trochu F. Compaction and creep behavior of glass reinforcement for liquid composites molding, Proceeding of ASM/EDS Advanced Composites Conference, Dearborn, Michigan, 1994: 357-367.

Figure captions

Figure 1. Two permeability measurement methods

(a) Discrete method for permeability measurement

(b) Continuous method for permeability measurement

Figure 2. Experimental device for permeability measurement

(a) Schematic diagram

(b) Photo view

Figure 3. Distribution of fiber volume fraction and pressure profile

(a) Discrete method (without fabric compaction)

(b) Continuous method (with fabric compaction)

Figure 4. Experimental results of permeability by the discrete method and by the continuous method

(a) Glass satin weave

(b) Carbon interlock weave

(c) Flax random mat

Figure 5. Numerical simulation procedure for permeability evaluation in the continuous method

Figure 6. Results of numerical simulations for permeability evaluation by the continuous method

(a) Glass satin weave (Q=5×10^{-7} m^3/s)

(b) Glass satin weave (Q=10^{-6} m^3/s)

(c) Glass satin weave (Q=2×10^{-6} m^3/s)

(d) Carbon interlock weave (Q=5×10^{-7} m^3/s)

(e) Carbon interlock weave (Q=10^{-6} m^3/s)

(f) Carbon interlock weave (Q=2×10^{-6} m^3/s)

(g) Flax random mat (Q=2×10^{-6} m^3/s)

(h) Flax random mat (Q=10^{-5} m^3/s)

(i) Flax random mat (Q=5×10^{-5} m^3/s)

Figure 7. Relative error against dimensionless number β

Figure 8. Fiber volume fraction against dimensionless number β

Table captions

Table 1. Model coefficients for fabric permeability and elastic deformation stress

	Equation (9)		Equation (10)	
	a [m^2]	b	c [Pa]	d
Glass satin weave	1.20×10^{-14}	-7.40	1.60×10^{8}	12.54
Carbon interlock weave	2.18×10^{-13}	-5.87	5.77×10^{7}	11.24
Flax random mat	4.55×10^{-13}	-2.57	2.77×10^{7}	3.98

Table 1.

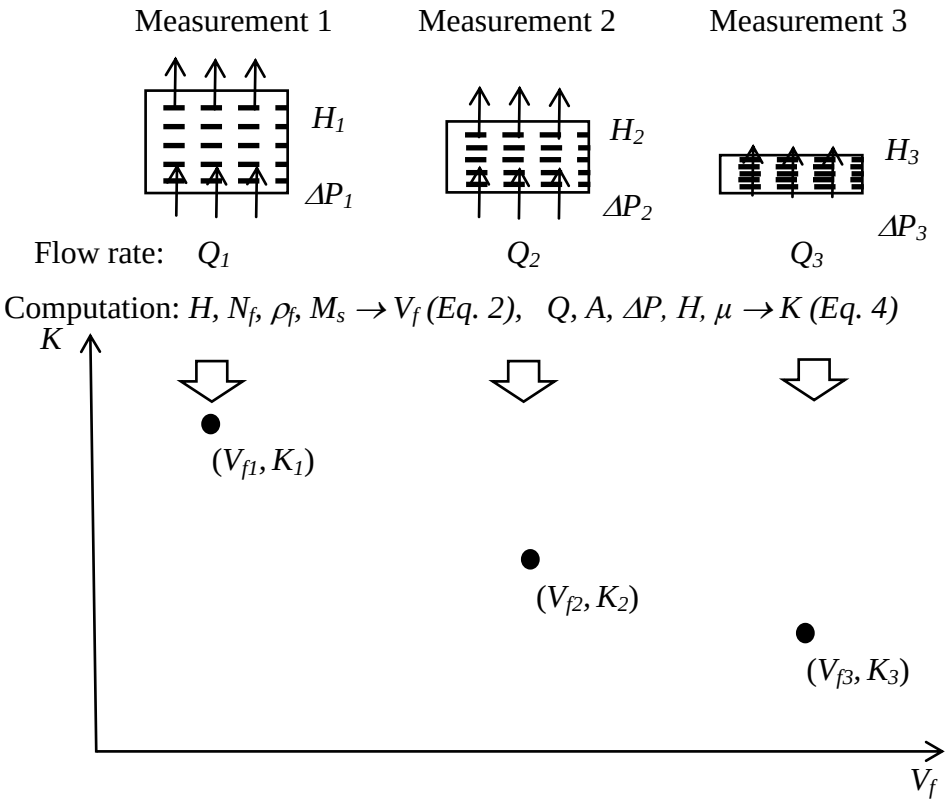

Figure 1.(a)

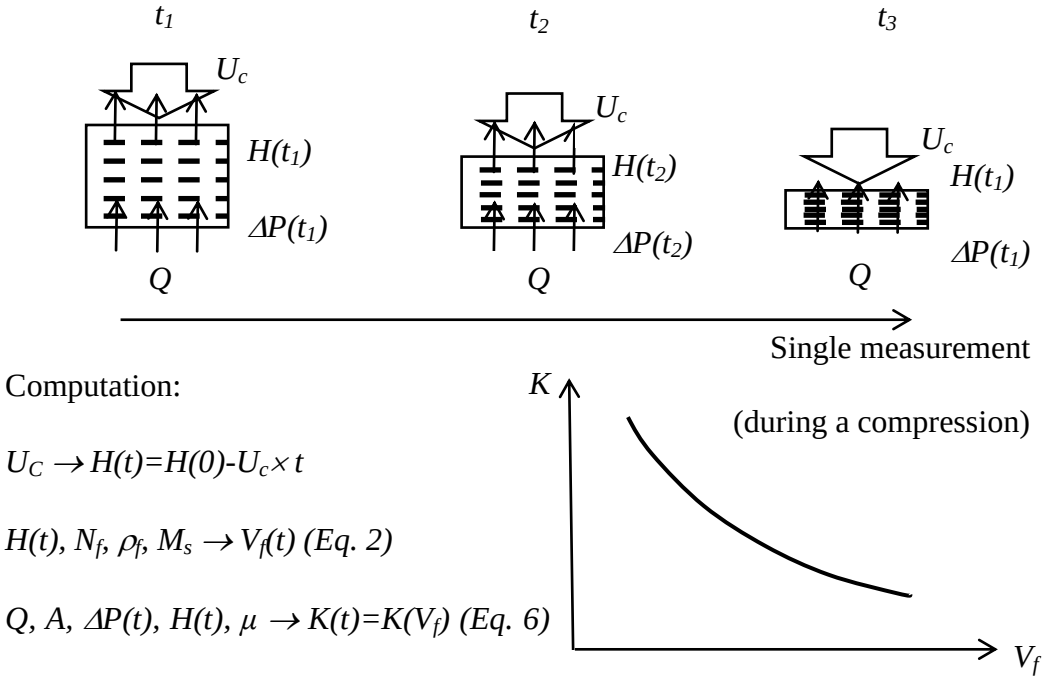

Figure 1.(b)

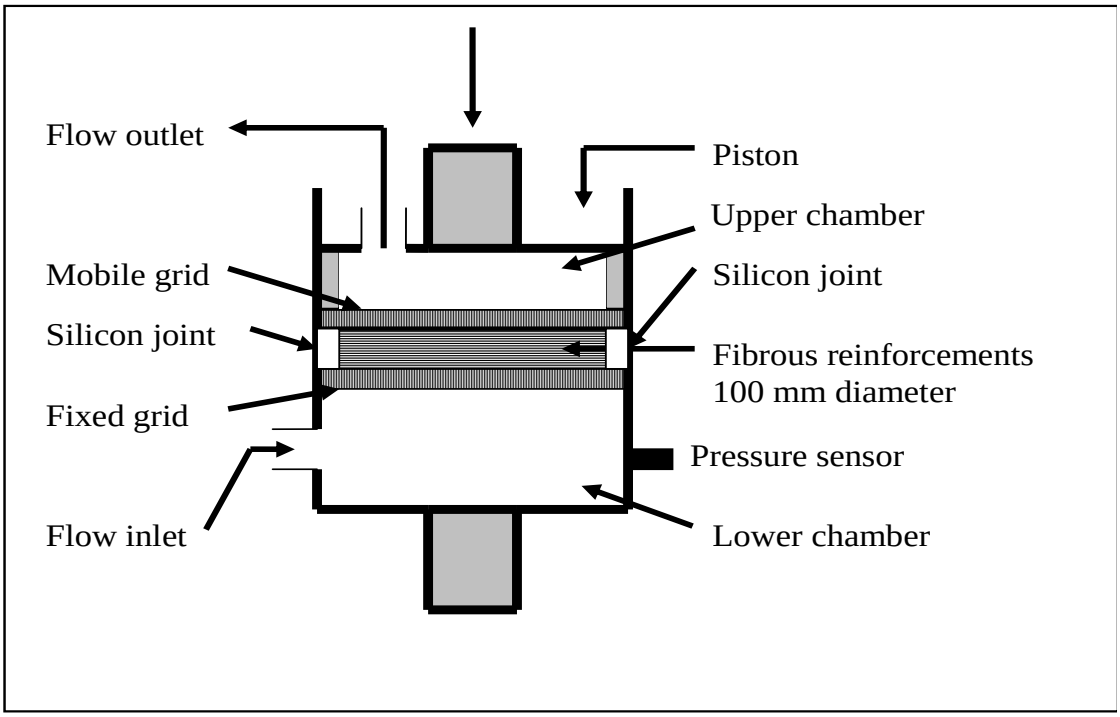

Figure 2 (a)

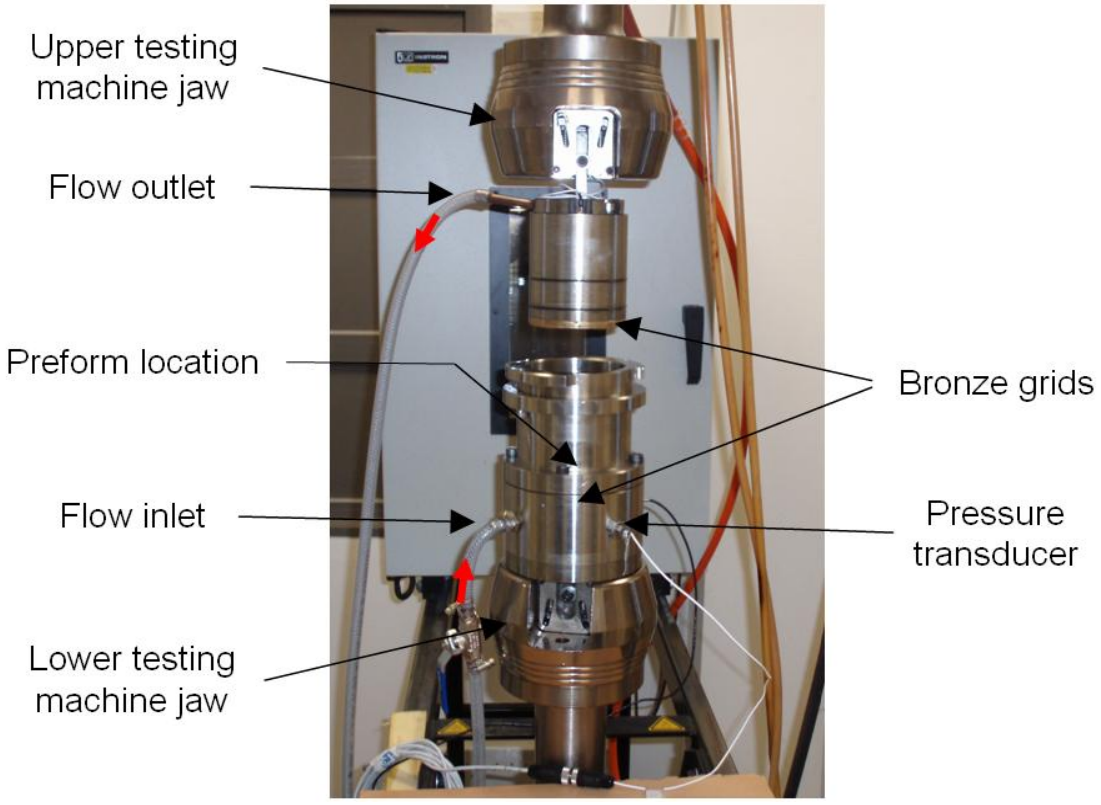

Figure 2 (b)

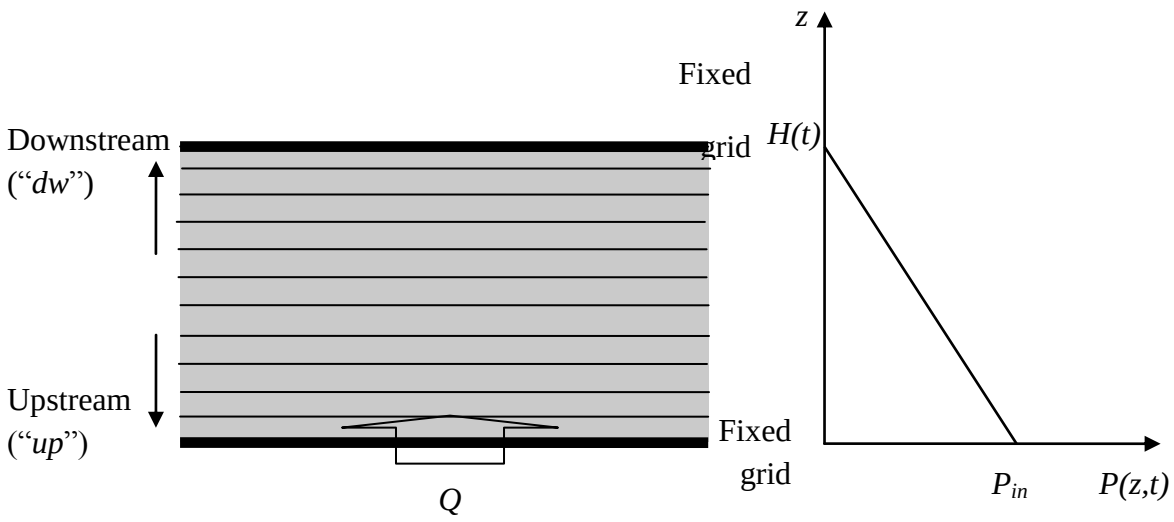

Fiber volume fraction: $V_{f,up} = V_{f,dw}$

Fiber velocity: $u_{f,up} = 0$, $u_{f,dw} = 0$

Figure 3 (a)

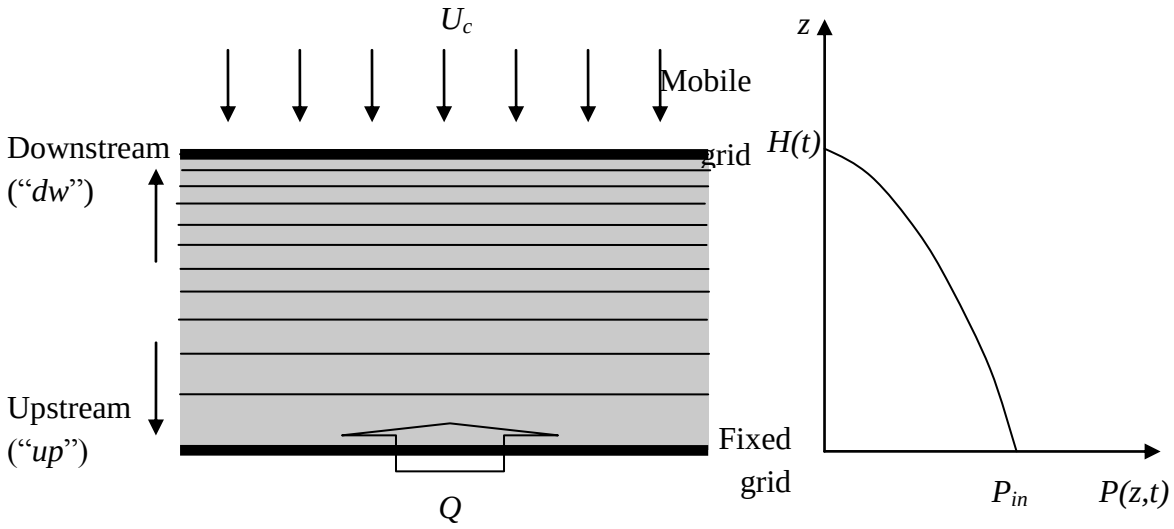

Fiber volume fraction: $V_{f,up} < V_{f,dw}$

Fiber velocity: $u_{f,up} = 0$, $u_{f,dw} = - U_c$

Figure 3 (b)

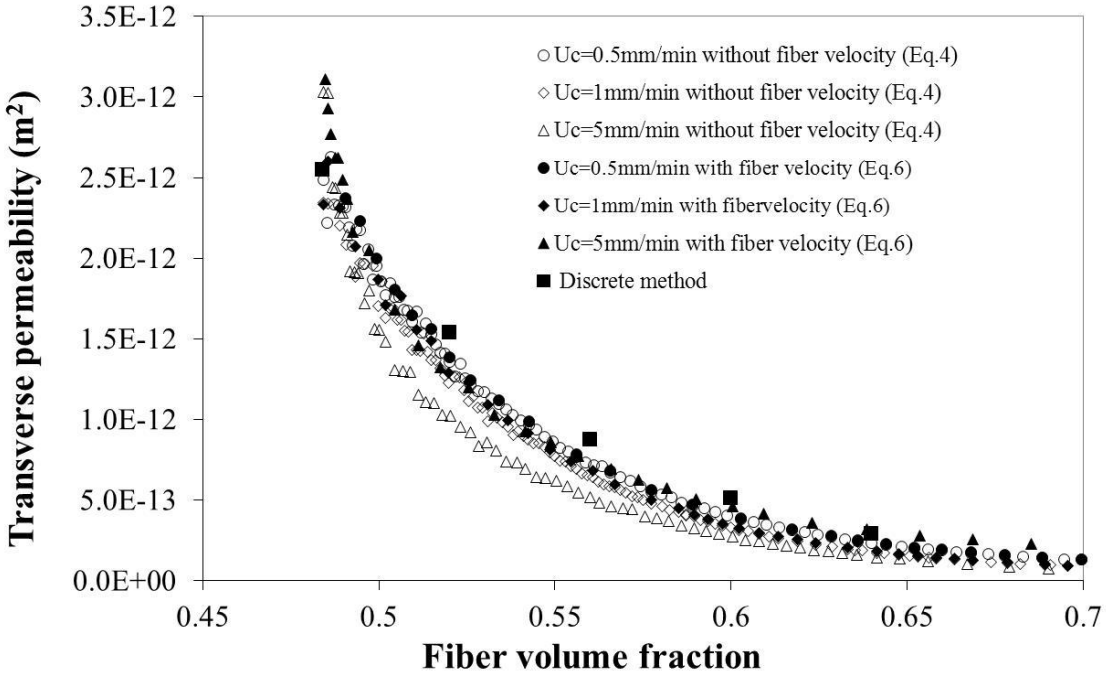

Figure 4 (a)

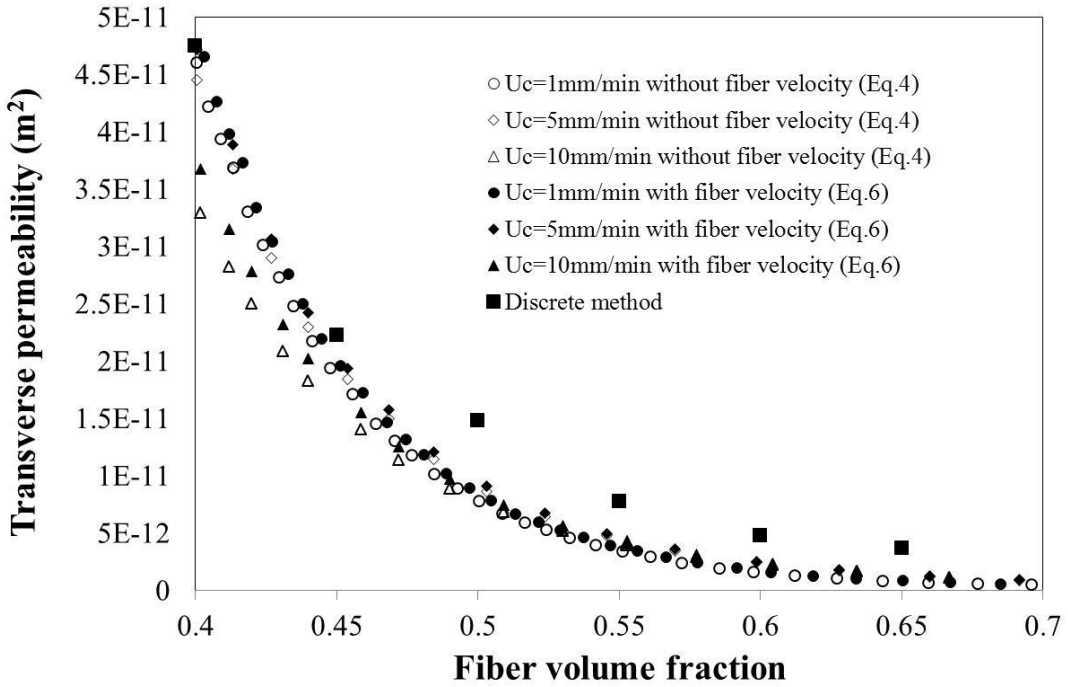

Figure 4 (b)

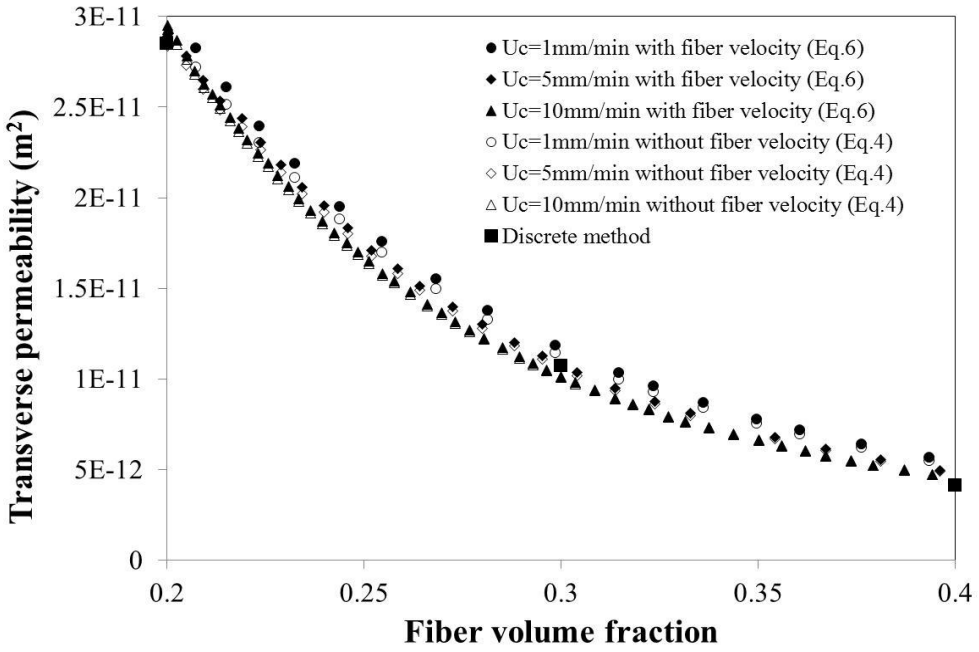
3E-11
2.5E-11
2E-11
1.5E-11
1E-11
5E-12
0
0.2
0.25
0.3
0.35
0.4
Transverse permeability (m²)
Fiber volume fraction
Uc=1mm/min with fiber velocity (Eq.6)
Uc=5mm/min with fiber velocity (Eq.6)
Uc=10mm/min with fiber velocity (Eq.6)
Uc=1mm/min without fiber velocity (Eq.4)
Uc=5mm/min without fiber velocity (Eq.4)
Uc=10mm/min without fiber velocity (Eq.4)
Discrete method

Figure 4 (c)

Input: U_c, Q, K_d, σ_f

Simulation: $H(t)$, $P(z,t)$, $V_f(z,t)$

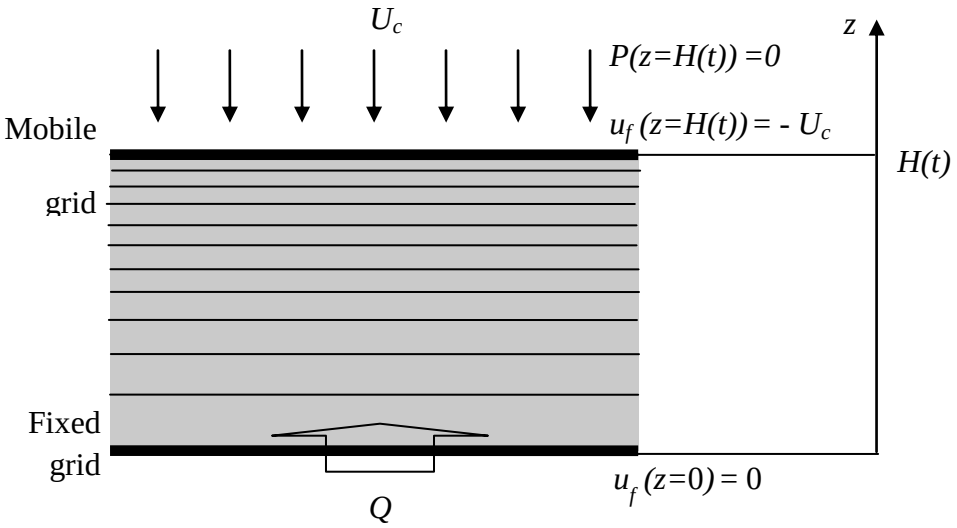

Output data: $P_{in}(z=0,t)$

Permeability evaluation: $V_{f,ave}(t)$ (Eq. 2) and $K_c(t)=K_c(V_{f,ave})$ (Eq. 6)

Figure 5

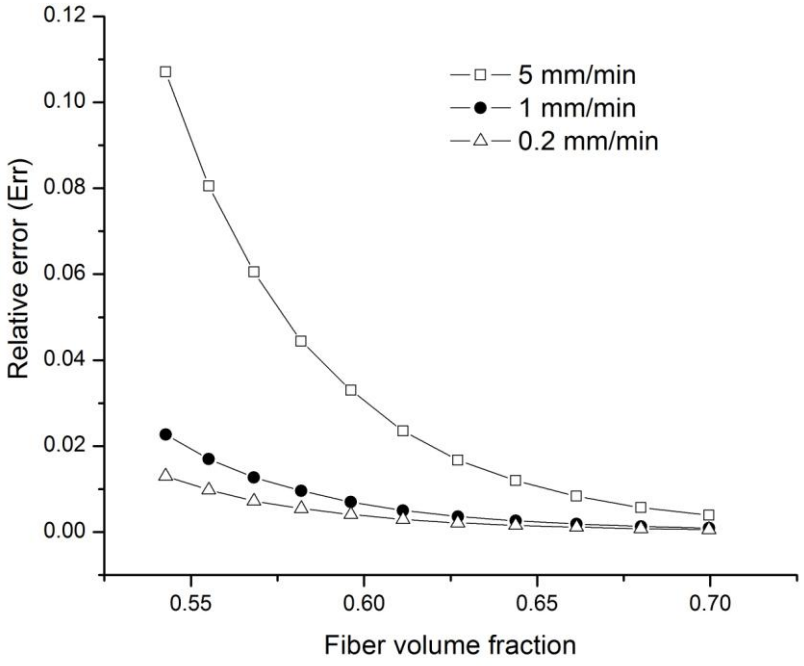

Figure 6 (a)

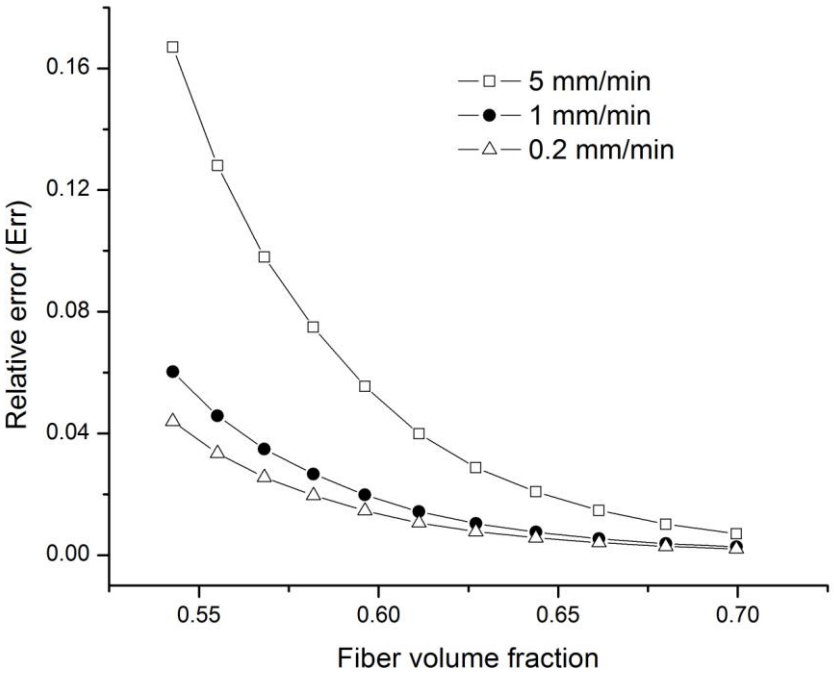

Figue 6 (b)

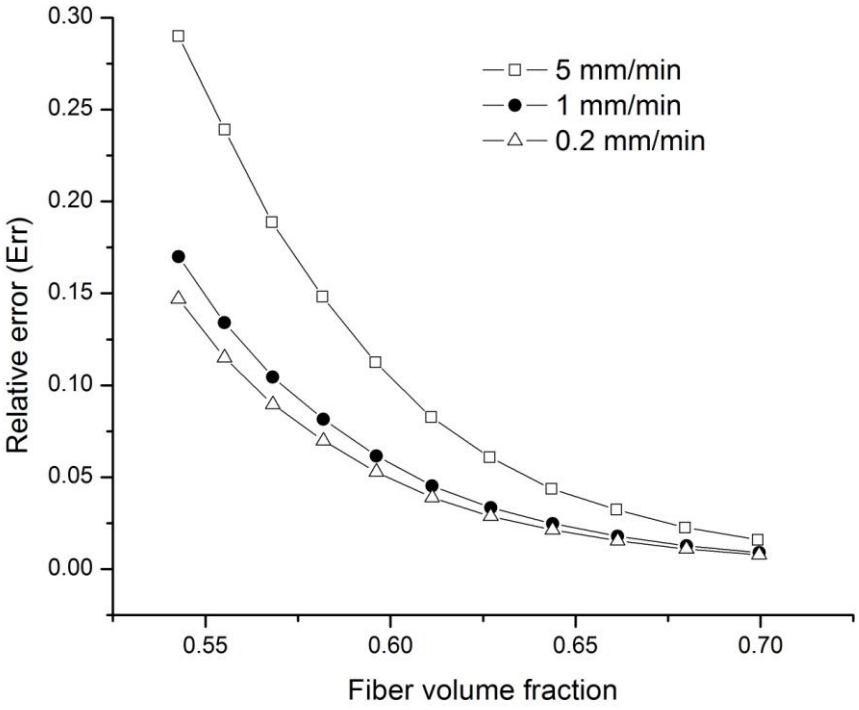

Figure 6 (c)

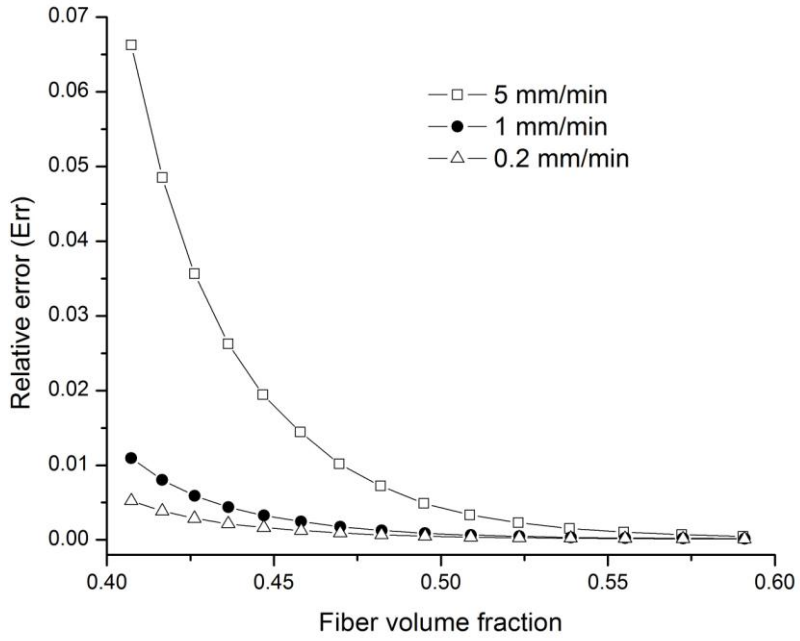

Figure 6 (d)

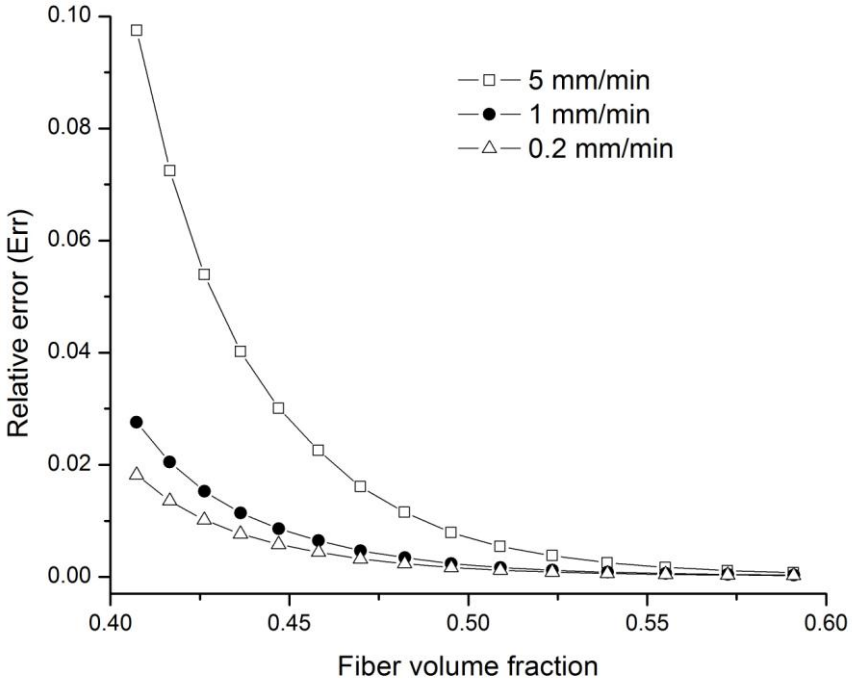

Figure 6 (e)

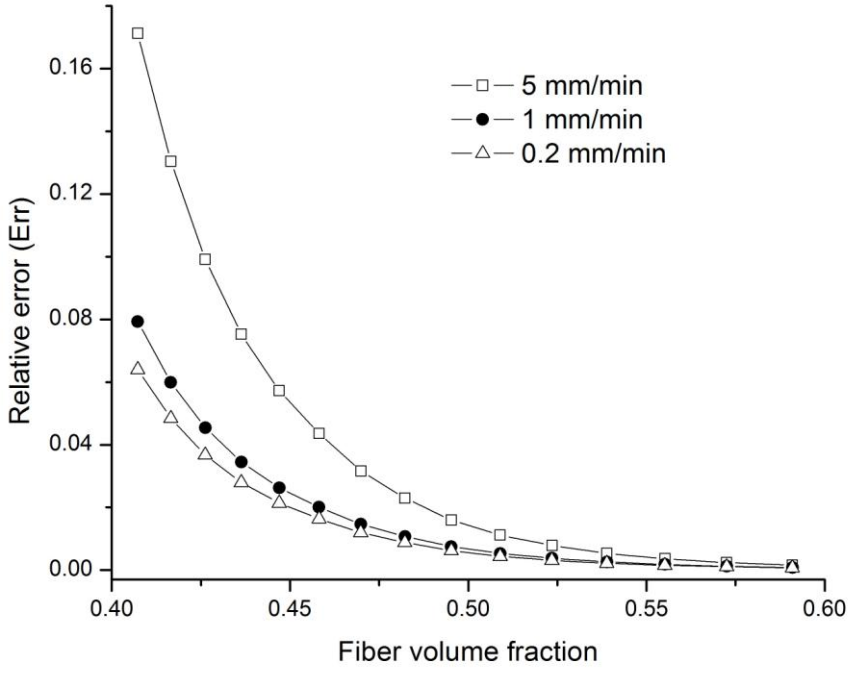

Figure 6 (f)

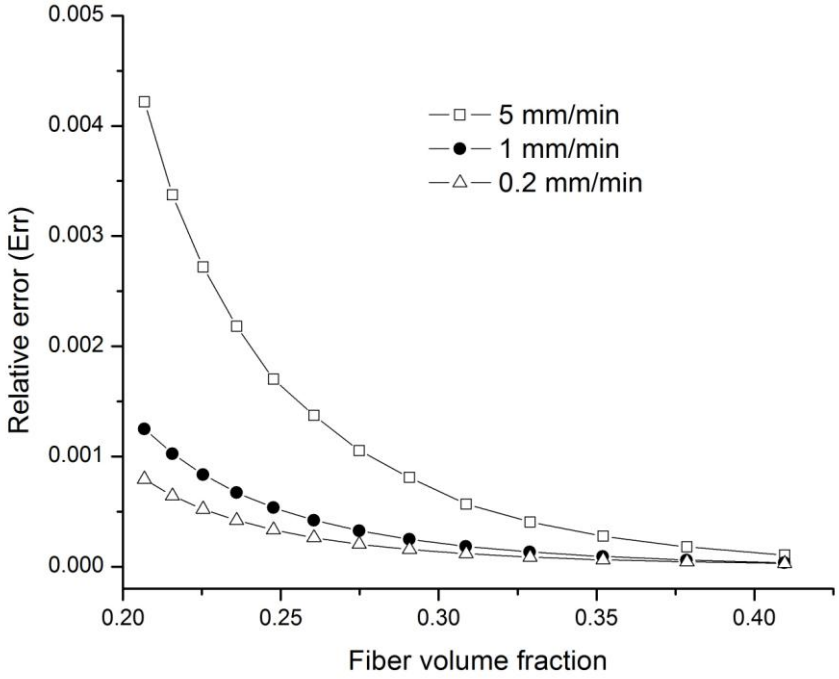

Figure 6 (g)

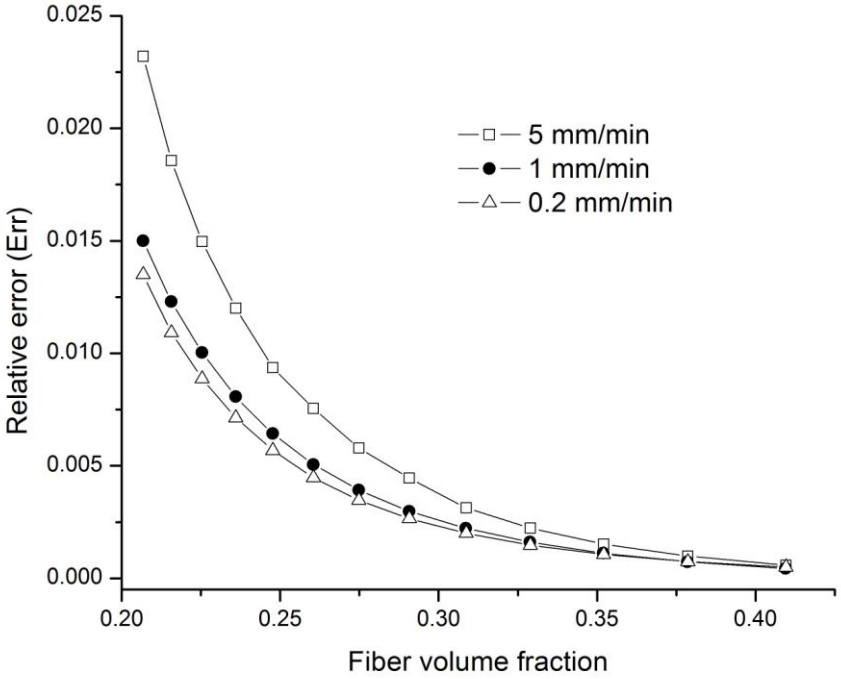

Figure 6 (h)

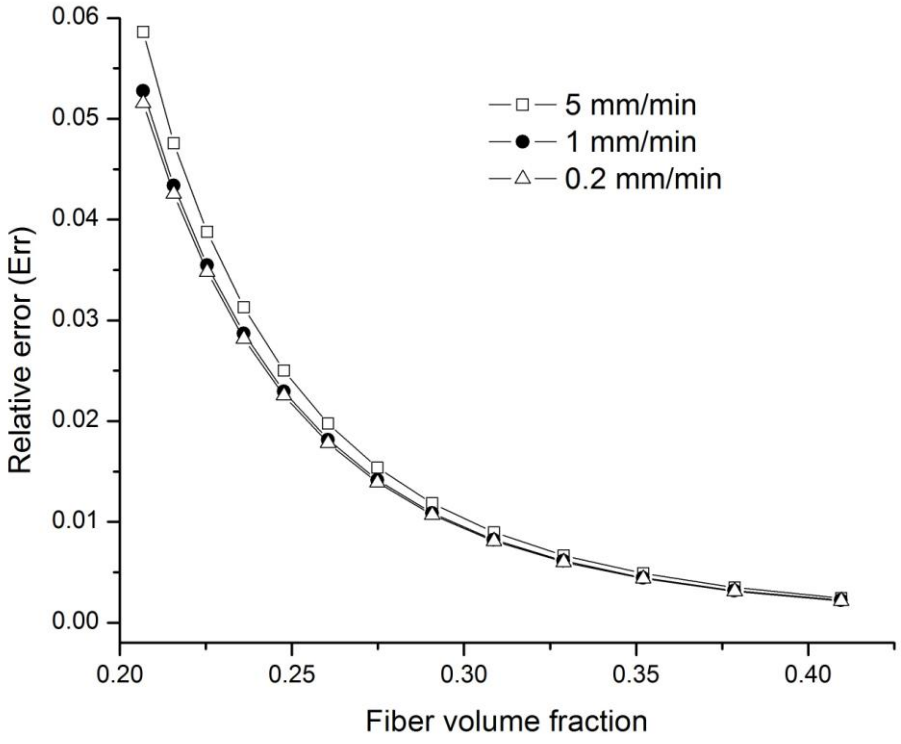
0.06
0.05
0.04
0.03
0.02
0.01
0.00
Relative error (Err)
0.20
0.25
0.30
0.35
0.40
Fiber volume fraction
5 mm/min
1 mm/min
0.2 mm/min

Figure 6 (i)

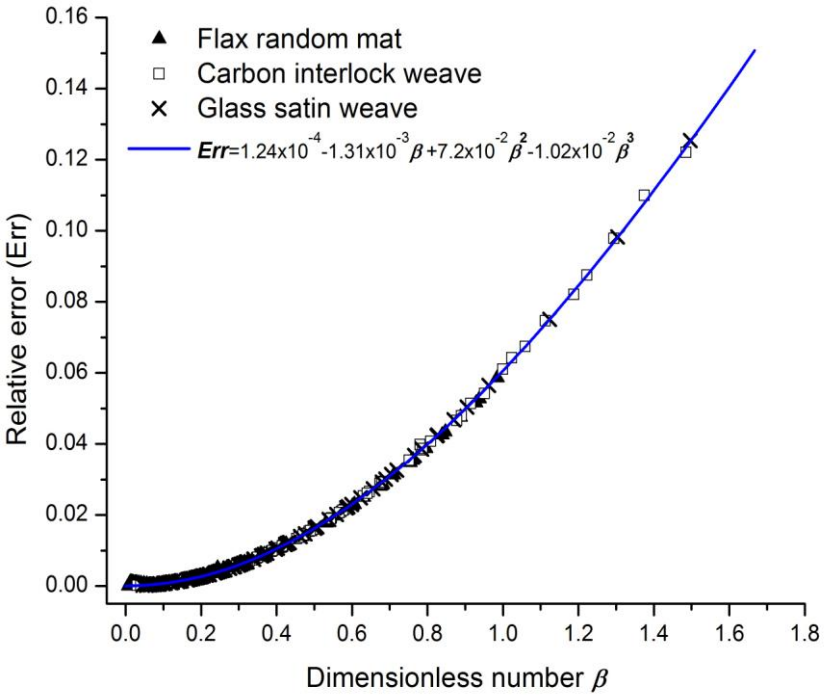

Figure 7.

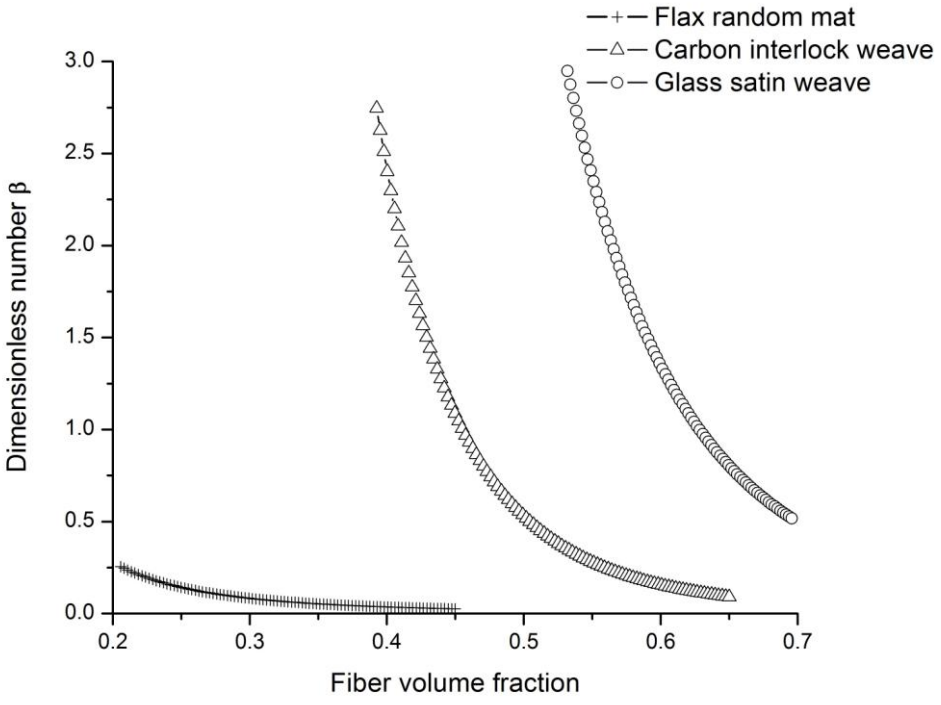

Figure 8.